Application of the LBM with adaptive grid on water hammer simulation

Ljubomir Budinski

ABSTRACT

A lattice Boltzmann method (LBM) is utilized to solve single-phase transient flow in pipes. In order to eliminate grid limitation related to the method of characteristics, governing equations are modified using appropriate coordinate transformation. The introduced modification removes connection between Courant number and spatial disposition of the computational nodes, forming a more flexible and robust mathematical base for numerical simulations. The computational grid is configured independently of the wave speed, significantly decreasing the demand for computational resources and maintaining the required accuracy of the method. Thereafter, the appropriate equilibrium distribution function for the D1Q3 lattice has been defined. In order to give a comprehensive base for modeling transient flow in complex pipeline systems, detailed elaboration of the corresponding boundary conditions has been given. Two benchmark problems with the corresponding error analysis are used to validate the proposed procedure.

Key words | adaptive grid, lattice Boltzmann method, partial differential equations, pressurized flow, transient flow, water hammer

Ljubomir Budinski
Faculty of Technical Sciences,
University of Novi Sad,
Trg Dositeja Obradovića 6,
Novi Sad 21000,
Serbia
E-mail: *ljubab@uns.ac.rs*

INTRODUCTION

Transition between two steady states in pipeline systems is a common phenomenon in engineering practice. Caused by sudden change in flow regime (pump failure, instantaneous valve closure), transient flow is characterized as highly unsteady flow with intensive pressure and velocity fluctuations, classically known as water hammer. In order to describe this phenomenon, a set of two hyperbolic partial differential equations, mass and momentum equation is utilized (Fox 1977; Wylie & Streeter 1978; Chaudhry 2014). Due to their hyperbolic nature, these equations are transformed to finite differential equations by using the method of characteristics (MC) (Wylie & Streeter 1978). Hartree (1958) was the first to introduce spatial interpolation in the case where the Courant number (Cr) was less than 1.0, while Wiggert & Sundquist (1977) and Vardy (1976) solved the pipeline transients for characteristics projecting over the fundamental grid size. Their analysis shows the effects of interpolation, spacing, and grid size on numerical attenuation and dispersion. Instead of widely used spatial interpolation, Goldberg & Wylie (1983) used interpolations in time, while Sibetheros *et al.* (1991) investigated the MC with spline polynomials for interpolations. Besides the MC, finite-difference (FD) and finite-volume (FV) methods have also been used in order to solve transient equations. Chudhury & Hussaini (1985) solved water hammer equations by MacCormack, Lambda, and Gabutti explicit FD schemes, while Verwey & Yu (1993) applied a space-compact high-order implicit scheme. Furthermore, Zhao & Ghidaoui (2004) formulated, applied, and analyzed first- and second-order explicit FV Godunov-type schemes for water hammer problems, while Leon *et al.* (2007, 2008) and Leon & Oberg (2013) applied FV method on two-phase water hammer flows. Application of the MC is proven to be simple to code, is accurate and efficient. However, major drawbacks related to the MC arise in practical applications. Since the spatial disposition of computational

doi: 10.2166/hydro.2016.164

points Δx is limited to relation $\Delta x = a\Delta t$, where a is the propagation (wave) speed and Δt is time step, frequently a single value for Δx is adopted for the whole system, as being representative. This distance is often prescribed by the system configuration; distance between two inner boundary conditions (for example, two air chambers). Consequently, a long pipe section can impose a large number of computational points, which can greatly affect the efficiency of the method. On the other hand, if spatial or time interpolation is used, additional procedures are inevitably introduced, which again influence the stability and accuracy of the method (Vardy 1976; Wiggert & Sundquist 1977; Goldberg & Wylie 1983).

In order to somehow overcome deficiencies related to the previously described methods, a lattice Boltzmann method (LBM) (Wolf-Gladrow 2005) is offered as an alternative approach. The first application of the LBM on transient flow was considered by Cheng *et al.* (1998), while only a case of rather simple practical implementation was done by Wu *et al.* (2008). In this paper, further development of the LBM is considered. In order to enhance the efficiency of the method, adaptive grid procedure is introduced. With this modification, restriction between Cr and spatial step Δx is removed, and arbitrary grid configuration approach is established. Hence, the number of computation points now can be significantly reduced, which is a desirable feature for long pipe sections. The corresponding grid size accuracy analysis is also conducted. Furthermore, mathematical formulation of most used boundary conditions is presented in detail. Implementation of the basic pipeline elements to the lattice Boltzmann model, such as pump, air chamber, valve, expansion/contraction of pipes, branching of pipes, is elaborated from the distribution function point of view, and some simplifications are introduced. This will much enhance the applicability of the method, with the opportunity to efficiently simulate complex pipeline systems. In contrast to the few lattice Bolzmann applications on transient flows available in the literature, where only the basics of the LBM are presented, the adaptive grid approach followed by detailed and comprehensive elaboration of the boundary condition and practical implementation offers scientists and engineers a robust and efficient tool for managing the transient flow in complex pipeline systems. The presented method was tested and verified on two different examples, while the MC was used for comparison.

TRANSIENT FLOW EQUATIONS

In general, one-dimensional transient flow is described by a set of two partial differential equations, namely the mass and momentum equation (Fox 1977; Chaudhry 2014):

$$\frac{\partial \Pi}{\partial t} + \frac{a^2}{g}\frac{\partial V}{\partial x} = 0, \tag{1}$$

$$\frac{\partial V}{\partial t} + g\frac{\partial \Pi}{\partial x} + \frac{\lambda}{2D}V|V| = 0. \tag{2}$$

In the above equations, t is time, x is Cartesian coordinate, Π is hydraulic head, V is longitudinal mean velocity, g is gravitational acceleration, and λ is friction factor. Wave speed a is defined as:

$$a^2 = \frac{K/\rho}{1 + \frac{K}{E}\frac{D}{e}c_1}, \tag{3}$$

where K is bulk modulus, E is Young's modulus, ρ is volumetric mass density and e is wall thickness. Depending on the pipe anchors, parameter c_1 is calculated as:

1. $c_1 = 1 - \mu/2$ – pipe anchored upstream,
2. $c_1 = 1 - \mu^2$ – pipe anchored throughout (no axial dilatation),
3. $c_1 = 1$ – expansion joints (axial dilatation allowed),

where μ is Poisson's coefficient.

In order to establish a base for adaptive grid procedure, Equations (1) and (2) are further transformed to the alternative coordinate system using the basic rules of coordinate transformation (Simmonds 1994):

$$\frac{\partial \Pi}{\partial t} + \frac{Ga^2}{g}\frac{\partial V}{\partial \zeta} = 0, \tag{4}$$

$$\frac{\partial V}{\partial t} + gG\frac{\partial \Pi}{\partial \zeta} + \frac{\lambda}{2D}V|V| = 0. \tag{5}$$

In Equations (4) and (5), ζ represents a new coordinate, while term $G = \partial\zeta/\partial x$ denotes corresponding basis. This formulation enables calculation conducted in equidistant ζ grid frame, imposed by the symmetry of the LBM.

LATTICE BOLTZMANN MODEL

In this paper, a D1Q3 lattice Boltzmann Bhatnagar–Gross–Krook model (LBGK) (Bhatnagar *et al.* 1954) is utilized. The evolution equation is defined as:

$$f_\alpha(\zeta + e_\alpha\Delta t, t + \Delta t) = f_\alpha(\zeta, t) - \frac{1}{\tau}(f_\alpha - f_\alpha^{eq}) + \frac{\Delta t}{e_\alpha}F_\alpha, \tag{6}$$

where f_α is the particle distribution function along the α link, f_α^{eq} is the local equilibrium distribution function, ζ is the position vector in the 1D domain, t is time, Δt is the time step, F_α is the force term, and τ is relaxation time. It should be noted that Equation (6) is defined using the new ζ-domain, therefore the required symmetry for discrete particle velocities e_α is ensured. For the three-velocity lattice, particle velocities e_α along the ζ direction are defined as $e_0 = 0$, $e_1 = \Delta\zeta/\Delta t$ and $e_2 = -\Delta\zeta/\Delta t$. Accordingly, $\Delta\zeta$ is lattice size in ζ direction.

In order to model transient flow equations using the corresponding LB method, appropriate equilibrium function f_α^{eq} is required. Using the form derived for 1D shallow water equations, introduced by Van Thang *et al.* (2010), the following formulation is proposed here:

$$f_\alpha^{eq} = \begin{cases} \left(\dfrac{1}{Ga^2} - \dfrac{G}{e^2}\right)g\Pi, & \alpha = 0 \\ \dfrac{V}{2e_\alpha} + \dfrac{gG}{2e^2}\Pi, & \alpha = 1, 2. \end{cases} \tag{7}$$

Term G in Equation (7) actually denotes connection between the physical and computational (lattice) domains, and it is calculated prior to the LBM computations. Furthermore, discrete formulation takes the form $G = \Delta\zeta/\Delta x$, where Δx is physical distance between computational nodes.

The last term in Equation (6) is the force term, and it is formulated as:

$$F_\alpha = -\frac{\lambda}{4D}V|V|. \tag{8}$$

In order to obtain second-order accuracy of the method, the force term is evaluated using the centered-scheme (Zhou 2004). Values are calculated at mid-point between the lattice points and its neighboring lattice points as:

$$F_\alpha = F_\alpha\left(\zeta + \frac{1}{2}e_\alpha\Delta t, t + \frac{1}{2}\Delta t\right). \tag{9}$$

Finally, the zeroth and first statistical moment is used to derive the corresponding hydraulic head Π and longitudinal velocity V:

$$\Pi(\zeta, t) = \frac{Ga^2}{g}\sum_\alpha f_\alpha(\zeta, t) = \frac{a^*}{g}\sum_\alpha f_\alpha(\zeta, t),$$
$$V(\zeta, t) = \sum_\alpha e_\alpha f_\alpha(\zeta, t). \tag{10}$$

Deduction of transient flow equations

To develop Equations (4) and (5), the Chapman–Enskog analysis (Wolf-Gladrow 2005) will be applied. By applying a Taylor series expansion in time and space around point (ζ, t) to the left side of Equation (6), and assuming $\Delta t = \varepsilon$, Equation (6) takes the form

$$\varepsilon\left(\frac{\partial}{\partial t} + e_\alpha\frac{\partial}{\partial\zeta}\right)f_\alpha + \frac{1}{2}\varepsilon^2\left(\frac{\partial}{\partial t} + e_\alpha\frac{\partial}{\partial\zeta}\right)^2 f_\alpha + O(\varepsilon^3) = F_\alpha\frac{\varepsilon}{e_\alpha} - \frac{1}{\tau}(f_\alpha - f_\alpha^{eq}). \tag{11}$$

Further, distribution function f_α is expressed as:

$$f_\alpha = f_\alpha^{(0)} + \varepsilon f_\alpha^{(1)} + \varepsilon^2 f_\alpha^{(2)} + O(\varepsilon^3), \tag{12}$$

while the centered scheme proposed by Zhou (2004) is used for the force term

$$F_\alpha = F_\alpha\left(\zeta + \frac{1}{2}e_\alpha\varepsilon, t + \frac{1}{2}\varepsilon\right), \tag{13}$$

which can also be written – via a Taylor expansion – as:

$$F_\alpha\left(\zeta + \frac{1}{2}e_\alpha\varepsilon, t + \frac{1}{2}\varepsilon\right) = F_\alpha(\zeta, t) + \frac{1}{2}\varepsilon\left(\frac{\partial}{\partial t} + e_\alpha\frac{\partial}{\partial\zeta}\right)F_\alpha + O(\varepsilon^2). \tag{14}$$

Substituting Equations (12) and (14) in Equation (11), the equation to order ε^0 is:

$$f_\alpha^{(0)} = f_\alpha^{eq}, \tag{15}$$

to order ε it is:

$$\left(\frac{\partial}{\partial t} + e_\alpha \frac{\partial}{\partial \zeta}\right) f_\alpha^{(0)} = -\frac{1}{\tau} f_\alpha^{(1)} + \frac{F_\alpha}{e_\alpha}, \tag{16}$$

and to order ε^2 it is:

$$\left(\frac{\partial}{\partial t} + e_\alpha \frac{\partial}{\partial \zeta}\right) f_\alpha^{(1)} + \frac{1}{2}\left(\frac{\partial}{\partial t} + e_\alpha \frac{\partial}{\partial \zeta}\right)^2 f_\alpha^{(0)} = -\frac{1}{\tau} f_\alpha^{(2)} + \frac{1}{2e_\alpha}\left(\frac{\partial}{\partial t} + e_\alpha \frac{\partial}{\partial \zeta}\right) F_\alpha. \tag{17}$$

Inserting Equation (16) into Equation (17) and then adding it to Equation (16) yields

$$\left(\frac{\partial}{\partial t} + e_\alpha \frac{\partial}{\partial \zeta}\right) f_\alpha^{(0)} + \varepsilon\left(1 - \frac{1}{2\tau}\right)\left(\frac{\partial}{\partial t} + e_\alpha \frac{\partial}{\partial \zeta}\right) f_\alpha^{(1)} = -\frac{1}{\tau}\left(f_\alpha^{(1)} - \varepsilon f_\alpha^{(2)}\right) + \frac{F_\alpha}{e_\alpha}. \tag{18}$$

Enforcing conditions $\sum_\alpha f_\alpha^{(n)} = 0$ and $\sum_\alpha e_\alpha f_\alpha^{(n)} = 0$ for $n \geq 1$, and taking the sum about α, Equation (18) takes the following form:

$$\frac{\partial}{\partial t}\sum_\alpha f_\alpha^{(0)} + \frac{\partial}{\partial \zeta}\sum_\alpha e_\alpha f_\alpha^{(0)} = \sum_\alpha \frac{F_\alpha}{e_\alpha}. \tag{19}$$

Evaluation of terms in the above equation using Equations (7), (8), and (10) results in the second-order accurate continuity equation (Equation (4)).

From $\sum e_\alpha \times$ Equation (18) about α we have

$$\frac{\partial}{\partial t}\sum_\alpha e_\alpha f_\alpha^{(0)} + \frac{\partial}{\partial \zeta}\sum_\alpha e_\alpha e_\alpha f_\alpha^{(0)} = \varepsilon\left(\tau - \frac{1}{2}\right)\frac{\partial}{\partial \zeta}\sum_\alpha e_\alpha e_\alpha \frac{\partial f_\alpha^{(1)}}{\partial \zeta} + \sum_\alpha F_\alpha. \tag{20}$$

Again, using Equations (7), (8), and (10) with the $\tau = 0.5$, results in the second-order accurate momentum equation (Equation (5)). Since the first term on the RHS actually denotes the second-order velocity derivative (diffusion), the τ parameter acts like an artificial viscosity which controls dispersion (oscillations) in the vicinity of the shocks.

Boundary conditions

Water supply systems are often characterized by a variety of elements (fittings, pumps, and storage tanks, etc.), hence adequate implementation of the boundary conditions represents one of the major tasks when transient pipe flow modeling is considered. Contrary to open channel flow cases, where formally only two types of boundary conditions are used, in transient pipe flow every type of element requires appropriate and specific LB formulation. Therefore, the detailed presentation of boundary conditions in the case of the transient LBM is presented in the following section.

Contraction/expansion of a pipe

In order to define contraction/expansion of a pipe as a boundary condition, equality of hydraulic heads Π (energy losses are neglected) and discharges Q between two boundary sections of the pipes P_j and P_{j+1} are used (Figure 1):

$$\Pi_{i=N,j} = \Pi_{i=1,j+1}, \tag{21}$$

$$Q_{i=N,j} = Q_{i=1,j+1}. \tag{22}$$

Index j denotes the corresponding pipe, while index $i = 1, \ldots, N$ marks the computational node along pipe j. It is obvious from Figure 1 that f_2 and f_1 are the unknown distribution functions related to pipes P_j and P_{j+1}, respectively. Introducing Equation (10) into Equations (21) and (22) and then expressing them in terms of unknown distribution

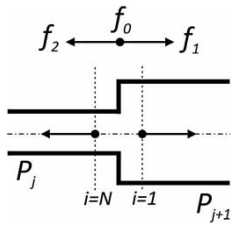

Figure 1 | Contraction/expansion of the pipe.

functions f_2 and f_1, respectively, gives

$$f_{2(i=N,j)} = \left(\frac{a^*_{j+1}}{a^*_j}\right)(f_0 + f_1 + f_2)_{(i=1,j+1)} - (f_0 + f_1)_{(i=N,j)}, \quad (23)$$

$$f_{1(i=1,j+1)} = \left(\frac{A_j}{A_{j+1}}\right)(f_1 + f_2)_{(i=N,j)} + f_{2(i=1,j+1)}, \quad (24)$$

where A is the cross section area of the corresponding pipe. Finally, substituting Equation (24) into Equation (23) leads to final expressions for calculating the unknown distribution functions in the forms

$$f_{2(i=N,j)} = \left\{\left(\left(\frac{A_j}{A_{j+1}}\right)f_{1(i=N,j)} + (f_0 + 2f_2)_{(i=1,j+1)}\right)\left(\frac{a^*_{j+1}}{a^*_j}\right) - (f_0 + f_1)_{i=N,j}\right\}\frac{1}{\left(1 + \frac{A_j}{A_{j+1}}\frac{a^*_{j+1}}{a^*_j}\right)}, \quad (25)$$

$$f_{1(i=1,j+1)} = \left(\frac{A_j}{A_{j+1}}\right)(f_1 - f_2)_{(i=N,j)} + f_{2(i=1,j+1)}. \quad (26)$$

It should be noted that Equations (25) and (26) are equally applicable for both cases, i.e., contraction and expansion, which makes them rather universal when change of pipe diameter is considered.

Valve

Opposite to pipe contraction/expansion, where energy losses are considered to be small (therefore neglected), a valve located at a particular node along a pipe (valve installed to the end of pipe is considered separately) can impose significant energy loss. Hence, in order to connect pipes P_j and P_{j+1} (Figure 2), the continuity and energy equation is utilized, respectively:

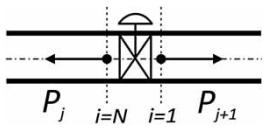

Figure 2 | Valve.

$$Q_{i=N,j} = Q_{i=1,j+1} = Q, \quad (27)$$

$$\Pi_{i=N,j} = \Pi_{i=1,j+1} \pm \xi_v \frac{Q^2}{A_v^2 2g}, \quad (28)$$

where ξ_v is loss coefficient and A_v is cross-sectional area of the pipe at the location of the valve. It should be noted that '±' in Equation (28) refers to direction of flow. Hence, the '+' sign denotes the case when flow is directed from pipe P_j to pipe P_{j+1}, while '−' refers to the opposite case. To define unknown distribution functions f_2 and f_1 corresponding to boundaries of pipes P_j and P_{j+1}, respectively, a similar procedure used in the contraction/expansion case will be applied. Furthermore, if the second term in Equation (28) is ignored, Equation (21) is obtained. Thus, in order to derive distribution functions at the location of the valve, the already defined form of Equation (25) is further modified, introducing the energy loss term

$$f_{2(i=N,j)} = \left\{\begin{array}{l}\left(\left(\frac{A_j}{A_{j+1}}\right)f_{1(i=N,j)} + (f_0 + 2f_2)_{(i=1,j+1)}\right)\left(\frac{a^*_{j+1}}{a^*_j}\right) \\ -(f_0 + f_1)_{i=N,j} \pm \frac{\xi_v}{A_v^2 2a^*_j}\left(A_j e(f_1 - f_2)_{(i=N,j)}\right)^2\end{array}\right\} \frac{1}{\left(1 + \frac{A_j}{A_{j+1}}\frac{a^*_{j+1}}{a^*_j}\right)}. \quad (29)$$

After some algebra, Equation (29) takes the form of a quadratic equation with solution in the form

$$f_{2(i=N,j)} = \frac{-b \pm \sqrt{b^2 - 4pc}}{2p}, \quad (30)$$

where

$$p = \pm\frac{\xi_v}{A_v^2}\frac{A_j^2 e^2}{2a^*_j},\ b = -\left(\pm 2\frac{\xi_v}{A_v^2}\frac{A_j^2 e^2}{2a^*_j}f_{1(i=N,j)} + 1 + \frac{A_j}{A_{j+1}}\frac{a^*_{j+1}}{a^*_j}\right),$$
$$c = \frac{a^*_{j+1}}{a^*_j}\left((f_0 + 2f_2)_{i=1,j+1} + \frac{A_j}{A_{j+1}}f_{1(i=N,j)}\right) - (f_0 + f_1)_{(i=N,j)} \pm \frac{\xi_v}{A_v^2}\frac{A_j^2 e^2}{2a^*_j}f^2_{1(i=N,j)}. \quad (31)$$

Next, the second unknown distribution function f_1 is obtained applying Equation (26).

Valve located at the end of the pipe

A special case of boundary condition is a valve located at the end of the pipe (Figure 3). Since the hydraulic head at the endpoint of the pipe coincides with the level of the outlet, Equation (28) consequently transforms into

$$\Pi_{i=N,j} = Z_v + \xi_v \frac{Q^2_{i=N,j}}{A_v^2 2g}. \tag{32}$$

Introducing Equation (10) into the above equation, the following form is obtained:

$$(f_0 + f_1 + f_2)_{(i=N,j)} = \left(Z_v + \frac{\xi_v}{A_v^2 2g} \left(A_j e (f_1 - f_2)\right)^2_{(i=N,j)} \right) \frac{g}{a_j^*}. \tag{33}$$

Since in this case f_2 is the only unknown distribution function (Equation (30)), Equation (33) again takes the form of a quadratic equation with the corresponding terms formulated as:

$$\begin{aligned} p &= -\frac{\xi_v}{A_v^2}\frac{A_j^2}{2a_j^*}e^2, \\ b &= \left(\frac{\xi_v}{A_v^2}\frac{A_j^2}{a_j^*}e^2\right) f_{1(i=N,j)} + 1, \\ c &= -Z_v \frac{g}{a_j^*} - \left(\frac{\xi_v}{A_v^2}\frac{A_j^2}{2a_j^*}e^2\right) f^2_{1(i=N,j)} + f_{1(i=N,j)} + f_{0(i=N,j)}. \end{aligned} \tag{34}$$

Branching pipes

In the case of branching pipes, a branch of four pipes with corresponding flow direction (see Figure 4) will be used as an example for derivation of the boundary condition. Hence, f_2 and f_1 are the unknown distribution functions related to the pair of pipes P_1–P_2 and P_3–P_4, respectively. In order to form

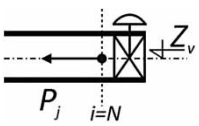

Figure 3 | Valve at the end of the pipe.

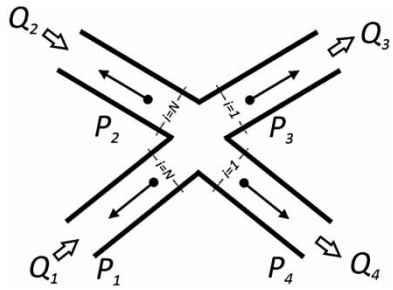

Figure 4 | Branch.

a boundary condition for a branch, a continuity equation along with hydraulic head equality between the pipes is utilized:

$$Q_1 + Q_2 = Q_3 + Q_4, \tag{35}$$

$$\Pi_1 = \Pi_2 = \Pi_3 = \Pi_4. \tag{36}$$

Further, introducing the first statistical moment

$$\begin{aligned} &-e\left(A_1 f_{2(N,1)} + A_2 f_{2(N,2)} + A_3 f_{1(1,3)} + A_4 f_{1(1,4)}\right) \\ &= -\underbrace{e\left(A_1 f_{1(N,1)} + A_2 f_{1(N,2)} + A_3 f_{2(1,3)} + A_4 f_{2(1,4)}\right)}_{C_1}, \end{aligned} \tag{37}$$

implementation of the corresponding zeroth moment into Equation (36) yields

$$\begin{aligned} \Pi_1 = \Pi_2 &\Rightarrow a_1^* f_{2(N,1)} - a_2^* f_{2(N,2)} \\ &= \underbrace{-a_1^*(f_0 + f_1)_{(N,1)} + a_2^*(f_0 + f_1)_{(N,2)}}_{C_2}, \\ \Pi_2 = \Pi_3 &\Rightarrow a_2^* f_{2(N,2)} - a_3^* f_{1(1,3)} \\ &= \underbrace{-a_2^*(f_0 + f_1)_{(N,2)} + a_3^*(f_0 + f_2)_{(1,3)}}_{C_3}, \\ \Pi_3 = \Pi_4 &\Rightarrow a_3^* f_{1(1,3)} - a_4^* f_{1(1,4)} \\ &= \underbrace{-a_2^*(f_0 + f_2)_{(1,3)} + a_4^*(f_0 + f_2)_{(1,4)}}_{C_4}. \end{aligned} \tag{38}$$

Finally, Equations (37) and (38) are written in matrix form:

$$\begin{bmatrix} A_1 e & A_2 e & A_3 e & A_4 e \\ a_1^* & -a_2^* & 0 & 0 \\ 0 & a_2^* & -a_3^* & 0 \\ 0 & 0 & a_3^* & -a_4^* \end{bmatrix} \begin{bmatrix} f_{2(N,1)} \\ f_{2(N,2)} \\ f_{1(1,3)} \\ f_{1(1,4)} \end{bmatrix} = \begin{bmatrix} C_1 \\ C_2 \\ C_3 \\ C_4 \end{bmatrix}, \tag{39}$$

while the solution is obtained using simple matrix inversion.

Reservoir located at the end of the pipe

Energy equation between the left reservoir, T, providing constant hydraulic head, and cross section $i = 1$ of the pipe is introduced (Figure 5):

$$\Pi_T = \Pi_{(i=1,j)} + (1 + \xi_{in}) \frac{Q^2_{(i=1,j)}}{2gA_j^2}. \tag{40}$$

Applying zeroth moment for hydraulic head $\Pi_{(i=1,j)}$ and first moment for discharge $Q_{(i=1,j)}$ (Equation (10)), the following equation is derived:

$$\begin{aligned} &\frac{e^2}{2a_j^*}(1+\xi_{in})f^2_{1(i=1,j)} + \left(1 - \frac{e^2}{a_j^*}(1+\xi_{in})f_{2(i=1,j)}\right) f_{1(i=1,j)} \\ &- \frac{g}{a_j^*}\Pi_t + \frac{e^2}{2a_j^*}(1+\xi_{in})f^2_{2(i=1,j)} + (f_0 + f_2)_{(i=1,j)} \\ &= 0. \end{aligned} \tag{41}$$

It is evident that Equation (41) is quadratic; hence the solution for the unknown distribution function f_1 is defined as:

$$f_{1(i=1,j)} = \frac{-b + \sqrt{b^2 - 4pc}}{2p}, \tag{42}$$

where

$$\begin{aligned} p &= \frac{e^2}{2a_j^*}(1+\xi_{in}), \\ b &= 1 - 2p f_{2(i=1,j)}, \\ c &= -\frac{g}{a_j^*}\Pi_t + p f^2_{2(i=1,j)} + (f_0 + f_2)_{(i=1,j)}. \end{aligned} \tag{43}$$

Furthermore, for a reservoir located at the right end of the pipe, the same procedure is utilized. Using the energy equation in the form

$$\Pi_T = \Pi_{(i=N,j)} - (1 + \xi_{in}) \frac{Q^2_{(i=N,j)}}{2gA_j^2}, \tag{44}$$

the solution of the corresponding quadratic equation is defined as:

$$f_{2(i=N,j)} = \frac{-b + \sqrt{b^2 - 4pc}}{2p}, \tag{45}$$

where

$$\begin{aligned} p &= \frac{e^2}{2a_j^*}(1+\xi_{in}), \\ b &= 1 - 2p f_{1(i=N,j)}, \\ c &= -\frac{g}{a_j^*}\Pi_t + p f^2_{1(i=N,j)} + (f_0 + f_1)_{(i=N,j)}. \end{aligned} \tag{46}$$

Surge tank

To minimize and possibly eliminate surges produced by the water hammer effect, the surge tank is often used as a possible solution (Figure 6). Water from the system enters and leaves the tank according to the pressure difference between the tank and the pipe, hence relieving the system from the sharp and intensive pressure surges. In order to introduce the surge tank as a boundary condition, the following set of equations is utilized:

$$Q_t = Q_{i=N,j} - Q_{i=1,j+1}, \tag{47}$$

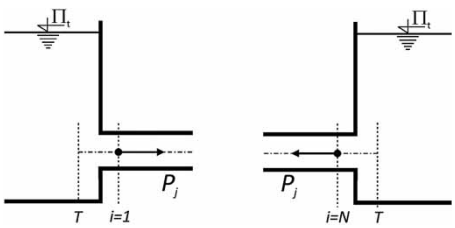

Figure 5 | Reservoir.

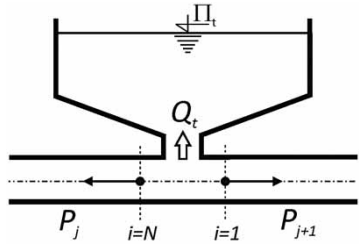

Figure 6 | Surge tank.

$$\Pi = \Pi_{i=N,j} = \Pi_{i=1,j+1} = \Pi_t \pm \xi_{pt}\frac{Q_t|Q_t|}{A_{pt}^2 2g}, \tag{48}$$

$$\frac{d\Pi}{dt} = \frac{Q_t}{A_t}. \tag{49}$$

where Q_t is flow in the tank, Π_t is hydraulic head inside the tank, A_t is cross-sectional area of the tank, ξ_{pt} is loss coefficient for the pipe–tank connection, and A_{pt} is cross-sectional area of the pipe connecting the tank and the system. Equations (47) and (48) represent continuity and energy equation between the tank and sections $(i = N, j)$ and $(i = 1, j + 1)$, respectively, while Equation (49) describes the connection between the flow and the hydraulic head inside the tank. Introducing the first statistical moment into Equation (47), and then eliminating the unknown distribution functions $f_{2(i=N,j)}$ and $f_{1(i=1,j+1)}$ from the equation using the zeroth statistical moment, connection between flow in the tank Q_t and hydraulic head in the pipe Π is derived:

$$Q_t = -\Pi eg\left(\frac{A_j}{a_j^*} + \frac{A_{j+1}}{a_{j+1}^*}\right) + A_j e(2f_1 + f_0)_{(i=N,j)} + A_{j+1}e(2f_2 + f_0)_{(i=1,j+1)}. \tag{50}$$

Further, combining Equation (50) with Equation (48), the quadratic equation is obtained:

$$\xi_{pt}\frac{Q_t|Q_t|}{A_{pt}^2 2g} + \left(Q_t - A_j e(2f_1 + f_0)_{(i=N,j)} - A_{j+1}e(2f_2 + f_0)_{(i=1,j+1)}\right) \frac{1}{eg\left(\frac{A_j}{a_j^*} + \frac{A_{j+1}}{a_{j+1}^*}\right)} + \Pi_t = 0. \tag{51}$$

Finally, Equation (51) is solved using Equation (45), where

$$p = \frac{\xi_{pt}}{A_{pt}^2 2g},$$
$$b = \frac{1}{eg\left(\frac{A_j}{a_j^*} + \frac{A_{j+1}}{a_{j+1}^*}\right)},$$
$$c = -\left(A_j e(2f_1 + f_0)_{(i=N,j)} + A_{j+1}e(2f_2 + f_0)_{(i=1,j+1)}\right) \frac{1}{eg\left(\frac{A_j}{a_j^*} + \frac{A_{j+1}}{a_{j+1}^*}\right)} + \Pi_t. \tag{52}$$

For the hydraulic head in the tank Π_t, Equation (49) is utilized in the form

$$\Pi_t^{n+1} = \Pi_t^n + \frac{Q_t \Delta t}{A_t}. \tag{53}$$

Air chamber

Since surge tanks are mostly used as a solution in larger systems (power plants), for smaller water supply systems a more practical and profitable solution in the form of an air chamber is utilized (Figure 7). Practically, both approaches are based on the same procedure. In comparison with the surge tank, the air chamber uses air pressure to compensate pressure head in the open tank, therefore reducing dimensions and overall cost of the chamber. Hence, for the derivation of boundary conditions, a procedure similar to that used in the case of the surge tank has been applied. In order to introduce air chamber as a boundary condition, the following set of equations is utilized:

$$Q_c = Q_{i=N,j} - Q_{i=1,j+1}, \tag{54}$$

$$\Pi = \Pi_{i=N,j} = \Pi_{i=1,j+1} = \Pi_c \pm \xi_{pc}\frac{Q_c|Q_c|}{A_{pc}^2 2g}, \tag{55}$$

$$\frac{dH_c}{dt} = \frac{Q_c}{A_c}, \tag{56}$$

$$\frac{dV_a}{dt} = Q_c, \tag{57}$$

where Q_c is flow in the chamber, Π_c is hydraulic head inside the chamber, H_c is water level, V_a is air volume, A_c is

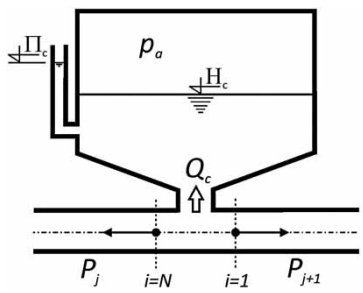

Figure 7 | Air chamber.

cross-sectional area of the chamber, ξ_{pc} is loss coefficient for the pipe–chamber connection, and A_{pc} is cross-sectional area of the pipe connecting the chamber and the system. Again, Equations (54) and (55) represent continuity and energy equation between the chamber and sections $(i = N, j)$ and $(i = 1, j + 1)$, respectively, while Equation (56) describes connection between the flow and the water level inside the chamber. Temporal change of air volume inside the chamber is defined by Equation (57). The hydraulic head in the chamber is formulated as:

$$\Pi_c = H_c + \frac{p_a}{\rho g}, \tag{58}$$

where p_a is air pressure, relationship between the pressure and air volume is required in order to close the system. For this, polytropic relation for ideal gas is used:

$$p_a^{abs} \cdot V_a^m = const, \tag{59}$$

where p_a^{abs} is absolute pressure ($p_a^{abs} = p_a + p_{atm}^{abs}$) and m is the polytropic index. Introducing the finite difference form of Equations (56) and (57) along with Equation (59) in to Equation (58), relation for the pressure head inside the chamber Π_c is obtained:

$$\Pi_c^{n+1} = H_c^n + \frac{Q_c^n \Delta t}{A_c} + \frac{const.}{\rho g\left(V^n - Q_c^n \Delta t\right)^m} - \frac{p_{atm}^{abs}}{g\rho}, \tag{60}$$

where n denotes time level. Further, combining Equation (50) – representing relationship between flow in the chamber Q_c and hydraulic head in the pipe Π – and Equation (60) with Equation (55), a quadratic equation similar to Equation (51) is derived:

$$\xi_{pc}\frac{Q_c|Q_c|}{A_{pc}^2 2g} + \left(Q_c - A_j e(2f_1 + f_0)_{(i=N,j)} - A_{j+1} e(2f_2 + f_0)_{(i=1,j+1)}\right) \frac{1}{eg\left(\frac{A_j}{a_j^*} + \frac{A_{j+1}}{a_{j+1}^*}\right)} + \Pi_c = 0. \tag{61}$$

Finally, solution is obtained using Equation (52) with the following replacements $\xi_{pt} = \xi_{pc}$, $A_{pt} = A_{pc}$ and $\Pi_t = \Pi_c$.

Pump

Pump failure is seen as the most common reason for inducing water hammer effect, hence pump has been incorporated into the transient LB model as the last possible form of boundary condition. For this purpose, the configuration in Figure 8 is utilized. In order to define unknown distribution functions $f_{2(i=N,j)}$ and $f_{1(i=1,j+1)}$, continuity and energy equations are defined:

$$Q_{i=N,j} = Q_{i=1,j+1} = Q, \tag{62}$$

$$\Pi_{(i=N,j)} + H_p - \xi_v \frac{Q|Q|}{A_v^2 2g} = \Pi_{(i=1,j+1)}. \tag{63}$$

In the above equation H_p represents total head developed by the pump, defined by the well-known four quadrants Suter relations (Wylie & Streeter 1978):

$$H_p = H_{p,0}\left(\alpha^2 + v^2\right) WH\left(\pi + \tan^{-1}\frac{v}{\alpha}\right), \tag{64}$$

where $v = Q/Q_0$ and $\alpha = N/N_0$ are dimensionless flow and speed of rotation of the pump, respectively. Subscript '0' refers to rated conditions, usually those at the best efficiency point. Function $WH(\pi + \tan^{-1} v/\alpha)$ of the considered pump can be determined accomplishing measurements on the corresponding pump, utilizing the relationship

$$\frac{Q_1}{N_1 D_1^3} = \frac{Q_2}{N_2 D_2^3}, \tag{65}$$

stating the condition of identical capacity of two pumps. If rotational speed of the pump α is known (regular pump regime), Equations (62)–(64) close the system of equations. However, when pump failure occurs, α is unknown, hence an additional equation is required. For this purpose a

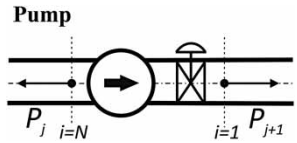

Figure 8 | Pump.

torque balance equation is used:

$$T_p - T_h = I\frac{d\omega}{dt}, \tag{66}$$

where T_p is the torque of the pump, T_h is the hydraulic torque, I is the moment of inertia of the pump and entrained liquid, and $d\omega/dt$ is the change in angular speed with time. It should be noted that in the case of pump failure the torque of the pump becomes zero instantaneously. By introduction of relations $\omega = N2\pi/60$ and $\beta = T/T_0$, Equation (66) can be discretized using the finite difference method as:

$$\frac{\alpha^{n+1} - \alpha^n}{\Delta t} = -\frac{15T_0}{\pi N_0 I}\left(\beta^{n+1} + \beta^n\right), \tag{67}$$

where β^{n+1} is derived applying the four quadrant relation in the form

$$\beta = \left(\alpha^2 + v^2\right)WB\left(\pi + \tan^{-1}\frac{v}{\alpha}\right). \tag{68}$$

The set of Equations (62), (63), (64), (67), and (68) close the system of required equations, which is then solved iteratively. The procedure is described here:

1. In the first step, functions $WH(\pi + \tan^{-1}v/\alpha)$ and $WB(\pi + \tan^{-1}v/\alpha)$ are determined using assumed values for v and α.
2. In the second step, dimensionless speed of rotation α^{n+1} and torque β^{n+1} is calculated using Equations (67) and (68), respectively.
3. Introducing the zeroth statistical moment in the form $\Pi(\zeta, t) = a^*/g\sum_{\alpha} f_\alpha(\zeta, t)$ into Equation (63), and using assumed value in the first iteration for the second unknown distribution function $f_{2(i=N,j)}$, in the third step the following equation is solved

$$\begin{aligned} f_{1(i=1,j+1)} &= -(f_0 + f_2)_{(i=1,j+1)} \\ &+ H_{p,0}\left(\alpha^2 + v^2\right)WH\left(\pi + \tan^{-1}v/\alpha\right)\frac{g}{a^*} \\ &- \xi_v v|v|\frac{Q_0^2}{2A_v^2 a^*} + (f_0 + f_1 + f_2)_{i=N,j}. \end{aligned} \tag{69}$$

4. In the fourth step, the second unknown distribution function $f_{2(i=N,j)}$ is calculated using the combination of Equation (62) and the first statistical moment

$$f_{2(i=N,j)} = f_{1(i=N,j)} - (f_1 - f_2)_{(i=1,j+1)}. \tag{70}$$

5. Finally, dimensionless flow $v = Q/Q_0$ is calculated using the distribution function from the previous step.
6. The entire procedure is repeated from stage 2 using tolerance $\Delta\alpha = 1.0 \times 10^{-6}$.

THE NUMERICAL SIMULATION AND THE VALIDATION OF THE MODEL

In order to test the proposed form of the LBM on more practical transient problems, we focus our test analysis mainly on the pump failure cases. Being the most common reason for inducing transient flows in pipeline systems, pump failure is, at the same time, complex enough and representative enough for testing the novel numerical method.

Single pipe system

For the first example a rather simple pipeline system is chosen (Figure 9). At the front end of the pipe, having length of $L = 2{,}000.0$ m, diameter $D = 0.90$ m, and friction factor $\lambda = 0.022$, one centrifugal pump (KRTK 500-630/908UNG-S) with actual flow rate $Q_0 = 2, 592.0$ m^3/h, actual developed head $H_{p,0} = 8.20$ m, efficiency $\eta = 78.5\%$, and speed of rotation $N_0 = 737$ rpm is set up (Amarex 2014). From the open reservoir, having water level $\Pi_R = 80.0$ m, water is pumped along the horizontal pipe vertically positioned at level $Z_p = 83.4$ m. Furthermore, two valves are implemented in the system. However, primarily the role of valves in this example is not flow regulation using an adapted closing dynamics, but rather boundary condition implementation on one hand (free outflow at the end of the pipe), and enforcement

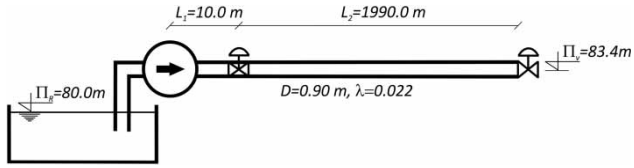

Figure 9 | Single pipeline system.

of the MC to define the computational grid along the pipe according to the smallest distance limitation (valve located $L_1 = 10.0$ m from the pump) on the other hand. As stated in the Introduction, MC utilizes an approach where the governing equations are solved along the characteristics (trajectories), which can connect two computational points ($Cr = 1.0$), or it can be projected outside ($Cr > 1.0$) or inside ($Cr < 1.0$) the computational cell. In order to avoid additional computational work and reduce numerical error (caused by interpolation) as much as possible, especially when non-linear definition $dx/dt = V \pm a$ for characteristic is used, most commercial softwares utilize a standard model, i.e., when $Cr = 1.0$. However, this approach also introduces a certain type of limitation if the computational grid is defined according to the smallest distance in the system. This can significantly increase dimension of the computational grid, which in turn influences overall computational efficiency. For the purpose of testing and verification of the transient LB method, a commercial software AFT Impulse 4.0 (Applied Flow Technology 2011) is used in our investigation.

Prior to the transient flow simulation, a steady flow state is established. For this purpose a classical energy equation is adopted. Applying the condition where the pump torque T_p is instantaneously reduced to zero, pump failure is induced and transient flow regime is obtained. As a consequence, intensive pressure and velocity variations are developed. In order to test the LBM for solving the transient equations (Equations (1) and (2)), comparison against the MC (AFT Impulse 4.0) is provided. For a control section, location at 1.500 m from the front end of the pipe is chosen. Comparison of the pressure and flow variations between the two methods is presented in Figure 10. Very good agreement between the compared models is achieved. Furthermore, in order to test stability of the LB procedure, related to the relaxation time τ, hydraulic grade-line corresponding to the extreme values (max/min) of hydraulic head is presented in Figure 11. It is evident from the presented figure that the change of the relaxation parameter does not affect the overall stability of the procedure, but small deviations between the compared results as well as between the two methods are present. Increase of the relaxation time parameter $\tau > 0.5$ introduces a second-order velocity derivative in the model through Equation (20), therefore differences in results of cases with different τ values may be explained as dissipation effects caused by this additional term acting like a

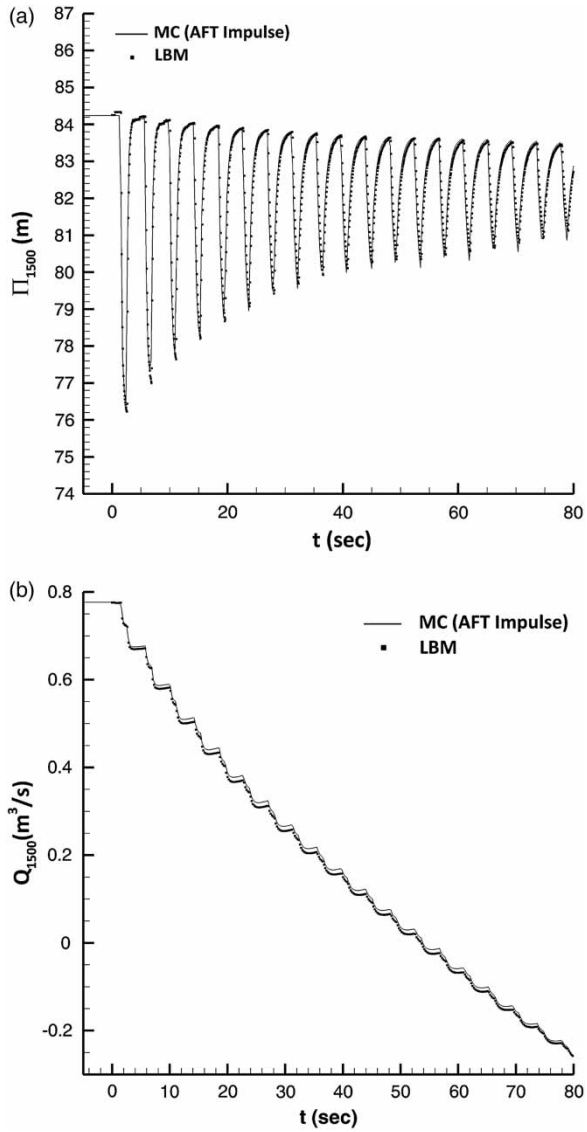

Figure 10 | Pump failure in a single pipeline system: (a) comparison of hydraulic head and (b) discharge obtained by the LBM and MC (AFT Impulse).

generator of artificial diffusion. Intensity of dissipation is presented in Figure 12. On the other hand, maximal difference between the LBM and MC, relative to the maximal drop of hydraulic head in the vicinity of the pump, is 3.125%.

The second part of the validation procedure includes grid-size analysis. In order to examine how the grid density affects the basic LBM indicators (in relation to the MC), primarily, efficiency and accuracy, four different cell size configurations $\Delta x = 10.0, 20.0, 40.0$ and 80.0 m have been adopted. This further produced one-dimensional computational grids with 201, 101, 51 and 26 computational points, while for time

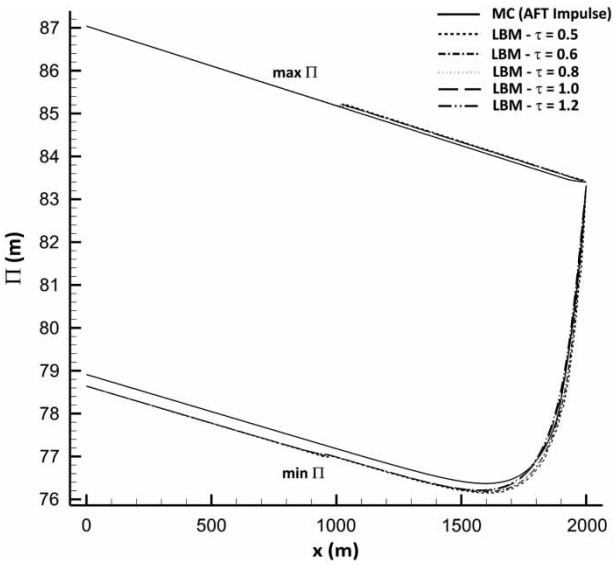

Figure 11 | *max*/*min* hydraulic grade-lines: comparison of the LBM with different relaxation time values to the MC (AFT Impulse).

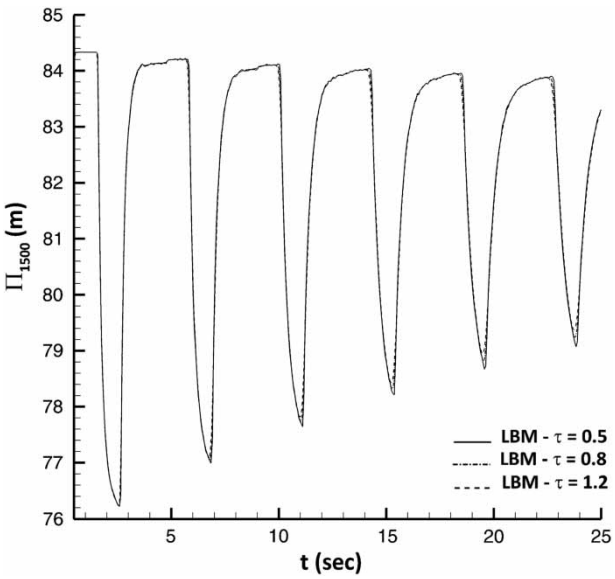

Figure 12 | Dissipation intensity caused by $\tau > 0.5$.

step, $\Delta t = 0.0100$, 0.0210, 0.0420 and 0.0800 have been used, respectively. For the MC, however, condition $Cr = 1.0$ is imposed by the system, which resulted in a grid size cell of $\Delta x = 10.0$ m (distance between the pump and valve is adopted as minimal length). Comparison of the results obtained for four different grid configurations with the MC is presented in Figure 13. It is evident from the figure that significant deviations between the compared results are notable only for $\Delta x = 80.0$ m, while for the finer grid sizes accuracy obtained for the finer grid ($\Delta x = 10.0$ m) is maintained.

A small pipeline system

To investigate water hammer effect using the proposed transient LB model in the case of complex pipeline configurations, for the second example the system presented in Figure 14 is utilized. Representing a 'real' practical problem, for which water hammer analysis is required, the chosen system is composed of five pipe sections (P), three branches (B), one air chamber (AC), one valve (V), and two centrifugal pumps (P_m) in parallel connection (same type of pump is used as in the previous example). All necessary parameters regarding the chosen system are depicted in Figure 14. After setting up the pipeline system, a computational grid with corresponding cell sizes Δx is established. In order to install the optimal number of computational points for each pipe section, different cell sizes are set for each pipe (see Figure 14). Hence, for the longest pipe P_5 cell size of $\Delta x = 72.87$ m is chosen, while for the shortest pipe $\Delta x = 10.00$ m is adopted. However, for MC the constant cell size of $\Delta x = 10.00$ is used. As a result, one-dimensional grids with 104 and 379 computational points are set for the LBM and MC, respectively.

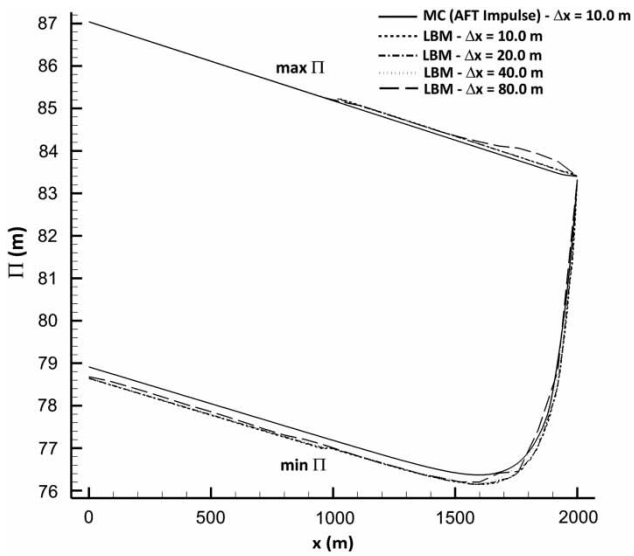

Figure 13 | *Max*/*min* hydraulic grade-lines: comparison of the LBM with different grid sizes to the MC (AFT Impulse).

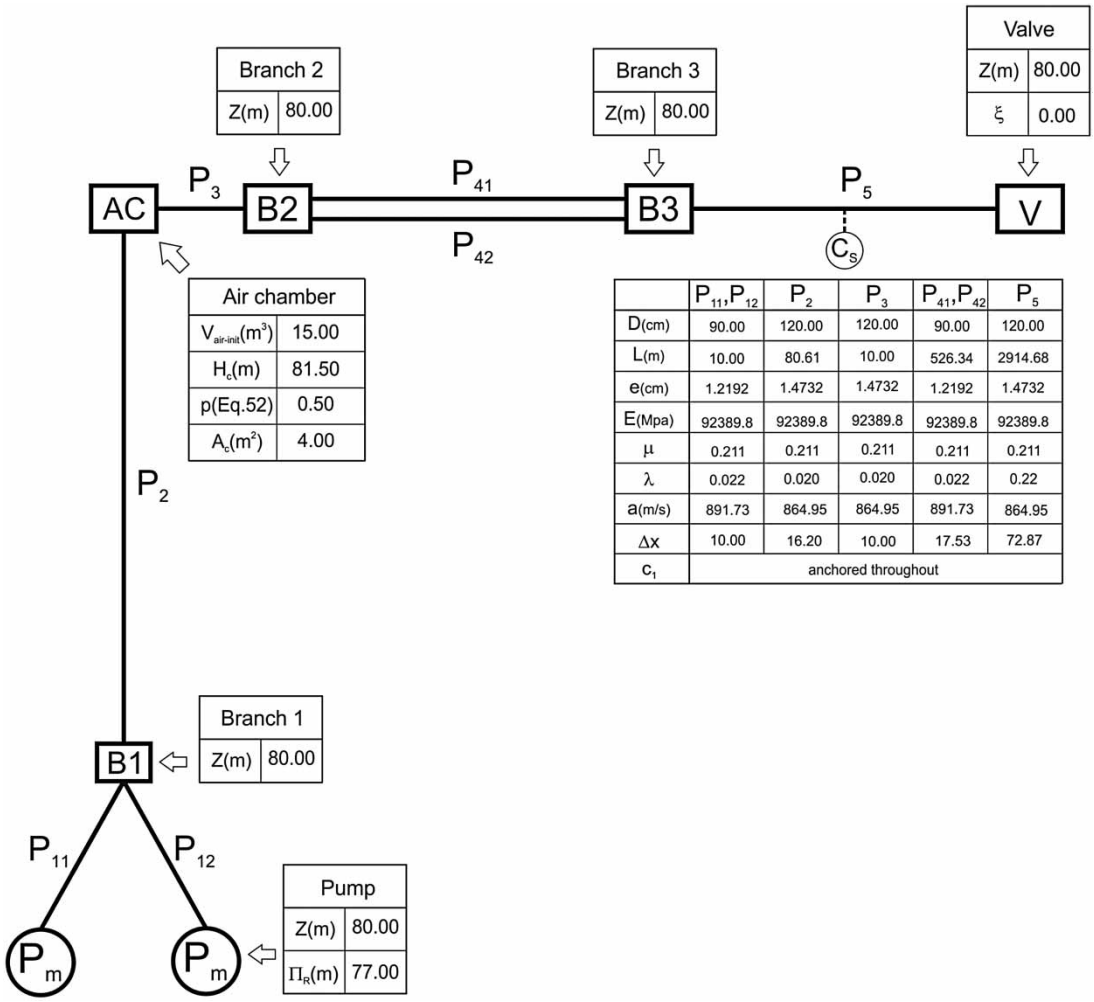

Figure 14 | Pipeline system configuration.

Two separate cases, with and without air chamber, are investigated. Similar to the previous example, initial conditions for both cases are derived using the classical energy equation. First, the case without air chamber is examined. For time step and relaxation time, values $\Delta t = 0.0120$ s and $\tau = 0.5030$ are adopted, respectively. Again, transient regime is induced by pump failure, i.e., instantaneously reducing torque T_p of both pumps to zero. This produces water hammer effect followed by intensive flow and pressure variations along the system. In order to compare results from the LBM and MC method, a control section located in the middle of pipe P_5 is chosen (C_S). Comparison of the obtained results in the form of hydraulic head variations and hydraulic grade-lines related to the extreme values (max/min) of hydraulic head is presented in Figures 15 and 16. Similar to the single pipe system, very good agreement between the two models is achieved. For the time variations of the hydraulic head (Figure 15), small deviations are present only at the local minimum, starting at $t = 30$ s. Relative to the maximal drop of hydraulic head, this digression falls in the range of $0.00 \div 3.77\%$. However, for the minimal and maximal extrema, i.e., for extreme pressure drops instantaneously after pump fails ($t = 13.8$ s in Figure 15), excellent agreement is obtained. Furthermore, this trend is relatively maintained along the whole system, which is shown in Figure 16. Only at a few computational points, located near the end of the system, is some divergence noted. Also, a 33.22% decrease in simulation time when the LB method is used is achieved. However, this model did not include additional procedures and coding for high performance computing (CUDA, OpenCL), which can further accelerate overall procedure metrics.

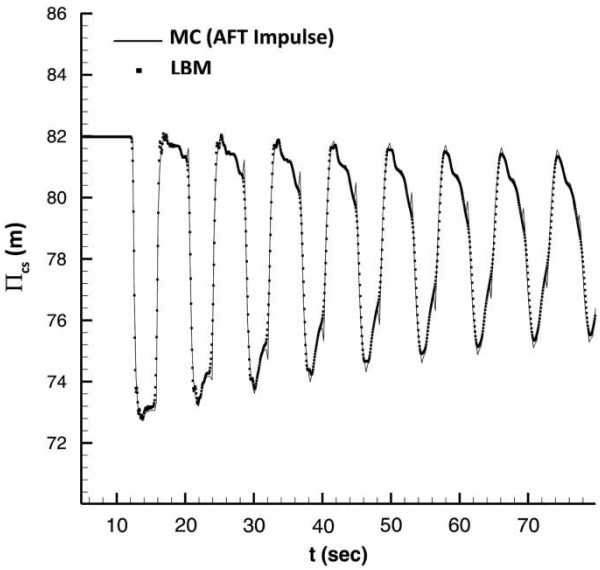

Figure 15 | Hydraulic head, comparison between LBM and MC (AFT Impulse).

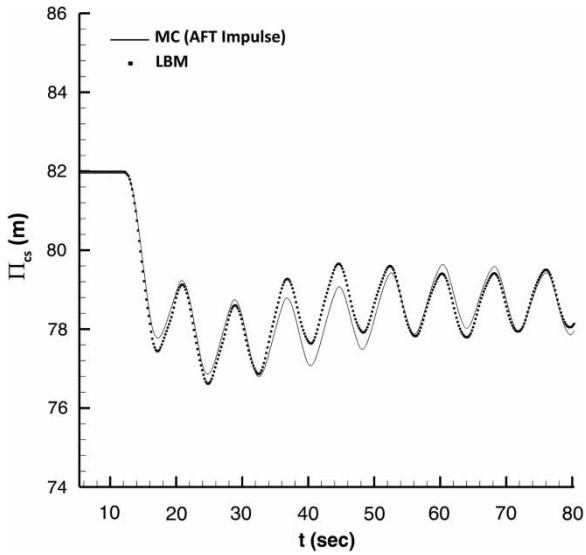

Figure 17 | Hydraulic head, comparison between LBM and MC (AFT Impulse) with an air chamber included.

Protection from high pressure oscillations using an air chamber is adopted and analyzed in the second step. To prevent severe damage of the pipeline system, caused by intensive pressure variations along the pipeline, an air chamber is installed 90.61 m downstream to the pump station (Figure 14). Installation of an air chamber into the LB model, setting the basic chamber parameters is required. The chamber is of cylindrical shape with diameter of $D_c = 4.0$ m, height $H = 2.5$ m. The initial water level of the chamber is set to $H_c = 81.50$ m, yielding initial air volume $V_{air-init} = 15.00\ \text{m}^3$. The chamber is connected to the system via a short pipe having loss coefficient $p = 0.50$, according to Equation (52). The same procedure of transient regime induction and analysis is applied here as in the previous example. Comparison of the results obtained by the LBM and MC in terms of hydraulic head variations and envelopes is given in Figures 17 and 18, respectively. Once again, very good agreement between the compared results

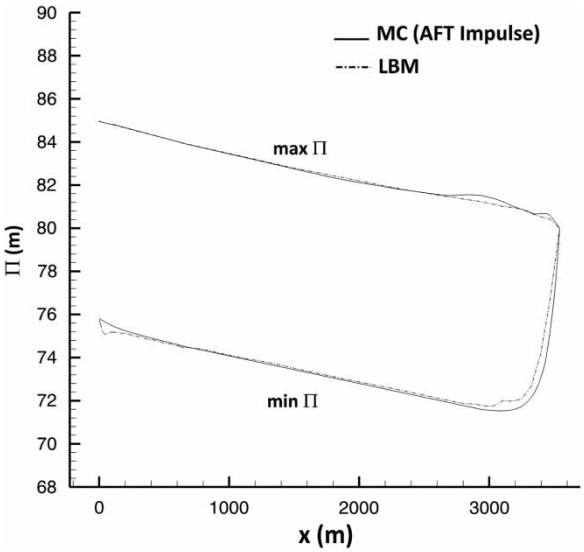

Figure 16 | *Max*/*min* hydraulic gradeline, comparison between LBM and MC (AFT Impulse).

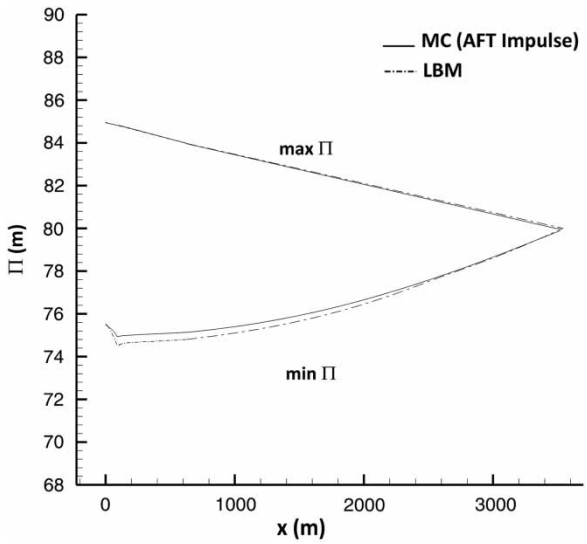

Figure 18 | *Max*/*min* hydraulic gradeline, comparison between LBM and MC (AFT Impulse) with an air chamber included.

is achieved in both cases. Minimal deviations noted in Figure 18, ranging from 0.0 ÷ 2.52% relative to the maximal head drop, demonstrate that the LBM model is more than capable for solving a variety of complex practical problems.

CONCLUSIONS

To overcome grid limitation typical to the MC, requiring Cr equal to one for stability in solving transient equations of pressurized flow, the same problem is solved by the LBM. To provide a higher level of flexibility in grid use, an adaptive grid approach is exploited. Sectional autonomy in the application of specific grid density to each pipe section significantly increases the efficiency of the overall procedure, maintaining the basic stability and accuracy. Introducing the LB method as an alternative to the MC in water hammer calculations provides the opportunity for parallel processing, which further increases the efficiency of calculations and cuts down calculation time. This is of high importance in large and complex pipeline systems. A detailed overview and elaboration of internal and external boundary conditions, i.e., pipeline elements and components is given. A real pipeline system with pump failure is modeled for the verification of the proposed LBM. Very good agreement with the MC is achieved.

REFERENCES

Amarex, K. R. T. 2014 http://www.ksb.com (last modified 18 December 2014).

Applied Flow Technology 2011 AFT Impulse Version 4.0, Colorado Springs, CO, USA (build date: 21 April 2011).

Bhatnagar, P. L., Gross, E. P. & Krook, M. 1954 A model for collision processes in gases: I. Small amplitude processes in charged and neutral one-component systems. *Phys. Rev.* **94**, 511–525.

Chaudhry, M. H. 2014 *Applied Hydraulic Transients*. 3rd edn. Springer, New York, p. 565.

Cheng, Y.-G., Zhang, S.-H. & Chen, J.-Z. 1998 Water hammer simulation by the Lattice Boltzmann method, transactions of the Chinese hydraulic engineering society. *J. Hydraul. Eng.* **6**, 25–31 (in Chinese).

Chudhury, M. H. & Hussaini, M. Y. 1985 Second-order accurate explicit finite-difference schemes for water hammer analysis. *J. Fluids. Eng.* **107**, 523–529.

Fox, J. A. 1977 *Hydraulic Analysis of Unsteady Flow in Pipe Networks*. Halsted Press, New York, p. 216.

Goldberg, D. E. & Wylie, B. 1983 Characteristics method using time-line interpolations. *J. Hydr. Div.* **109** (5), 670–683.

Hartree, D. R. 1958 *Numerical Analysis*. 2nd edn. Clarendon Press, Oxford.

Leon, A. S. & Oberg, N. 2013 *User's manual for Illinois Transient Model-two equation model v. 1.3. A Model for the Analysis of Transient Free Surface, Pressurized and Mixed Flows in Storm-Sewer Systems*. Oregon State University, Corvallis, OR.

Leon, A. S., Ghidaoui, M. S., Schmidt, A. R. & García, M. H. 2007 An efficient finite-volume scheme for modeling water hammer flows. In: *Contemporary Modeling of Urban Water Systems, Monograph 15* (W. James, ed). CHI, Guelph, Ontario.

Leon, A. S., Ghidaoui, M. S., Schmidt, A. R. & Garcia, M. H. 2008 An efficient second-order accurate shock-capturing scheme for modeling one and two-phase water hammer flows. *J. Hydraul. Eng.* **134** (7), 970–983.

Sibetheros, I. A., Holley, E. R. & Branski, J. M. 1991 Spline interpolations for water hammer analysis. *J. Hydraul. Eng.* **117** (10), 1332–1351.

Simmonds, J. G. 1994 *A Brief on Tensor Analysis*. Springer, New York, p. 112.

Van Thang, P., Chopard, B., Lefèvre, L., Ondo, D. A. & Mendes, E. 2010 Study of the 1D lattice Boltzmann shallow water equation and its coupling to build a canal network. *J. Comput. Phys.* **229**, 7373–7400.

Vardy, A. E. 1976 On the use of the method of characteristics for the solution of unsteady flows in networks. In: *Proceedings 2nd International Conference Pressure Surges*, London, UK, 1–4 January. BHRA Fluid Engineering, UK.

Verwey, A. & Yu, J. H. 1993 A space-compact high-order implicit scheme for water hammer simulations. In: *Proceedings of XXVth IAHR Congress*, Tokyo, Japan.

Wiggert, D. C. & Sundquist, M. J. 1977 Fixed-grid characteristics for pipeline transients. *J. Hydr. Div.* **103** (12), 1403–1416.

Wolf-Gladrow, D. A. 2005 *Lattice-Gas Cellular Automata and Lattice Boltzmann Models – An Introduction*. Springer-Verlag, Berlin, p. 266.

Wu, Y., Chi, L. & Zhang, H. 2008 Study of resistance distribution and numerical modeling of water hammer in a long-distance water supply pipeline. In: *Proceedings of the 10th Annual Water Distribution Systems Analysis Conference*, Kruger National Park, South Africa, 17–20 August. American Society of Civil Engineers, Reston, VA.

Wylie, E. B. & Streeter, V. L. 1978 *Fluid Transients*. McGraw-Hill Book Co, New York.

Zhao, M. & Ghidaoui, M. S. 2004 Godunov-type solutions for water hammer flows. *J. Hydraul. Eng.* **1130** (4), 341–348.

Zhou, J. G. 2004 *Lattice Boltzmann Methods for Shallow Water Flows*. Springer-Verlag, Berlin, p. 112.

First received 5 August 2015; accepted in revised form 24 November 2015. Available online 5 January 2016